

PROPERTIES OF LIGHT-EMITTING POROUS Si AND Si_{1-x}Ge_x ALLOYS
PRODUCED BY STAIN ETCHING

ROBERT W. FATHAUER

*Center for Space Microelectronics Technology, Jet Propulsion Laboratory,
California Institute of Technology, 4800 Oak Grove Dr., Pasadena, California 91109*

ABSTRACT

Porous Si can be produced in "stain" etches as well as by anodic etching. In the stain-etch case, the sample is simply immersed in a solution, most commonly consisting of HF, HNO₃, and H₂O. The resulting porous Si film is relatively thin and exhibits visible luminescence similar to that observed for anodically-etched Si. Stain etching provides greater flexibility than anodic etching in some cases, and has been used to produce light-emitting porous Si in selected areas. A variety of characterization tools have been employed to demonstrate that porous Si produced by stain etching is predominantly amorphous, though small crystallite have been observed near the interface with the substrate in some samples. Stain etching has also been used to produce porous Si_{1-x}Ge_x alloy layers from layers grown by molecular beam epitaxy. Using analytical electron microscopy techniques, the porosity, alloy composition, and impurity concentrations have been profiled as functions of depth in these layers. Luminescence from these layers is found to decrease dramatically with increasing Ge content, without significant shifting of the peak energy. Implications of these results for luminescence mechanisms are discussed.

Table of Contents

1. Introduction	
2. Production of Porous Silicon and $\text{Si}_{1-x}\text{Ge}_x$ Alloys by Stain Etching	
2.1. <i>Stain Etching of Silicon</i>	
2.2. <i>Stain Etching of $\text{Si}_{1-x}\text{Ge}_x$ Alloys</i>	
2.3. <i>Selective-area Production of Porous Silicon by Stain Etching</i>	
2.4. <i>Fabrication of Amorphous/Crystalline Superlattices by Stain Etching</i>	
3. Microstructural Properties	
3.1. <i>Surface Morphology</i>	
3.2. <i>Crystallinity</i>	
3.3. <i>Porosity</i>	
4. Composition and Chemical Properties	
4.1. <i>Elemental Composition</i>	
4.2. <i>Electronic Structure</i>	
5. Luminescence Properties	
5.1. <i>Photoluminescence</i>	
5.2. <i>Electroluminescence</i>	
6. Implications for Mechanism of Luminescence	
6.1. <i>Amorphous Nature of Porous Silicon Produced by Stain Etching</i>	
6.2. <i>Luminescence behavior of $\text{Si}_{1-x}\text{Ge}_x$ Alloys</i>	
7. Conclusions	
References	

1. Introduction

Porous Si has been studied at a low level for over 30 years,¹⁷ but there has been considerable activity recently due to the observation of strong visible luminescence at room temperature.¹⁸ Luminescent porous Si has been primarily produced by anodic etching of Si in concentrated (49%) hydrofluoric acid¹⁹ or solutions of HF in water,²⁰ ethanol,²¹ or acetic acid.²² Stain films on Si have been known for a comparable period of time,^{23,27} and have been shown to consist of porous material similar to that produced by electrochemical etching.²⁷ The most commonly used stain-etch solutions consist of HF:HNO₃:H₂O, though other oxidizers have been used as well.^{27,1}

Porous Si films produced by immersion in stain etches have been shown to exhibit similar luminescence to that observed for electrochemically etched films.^{1,3,9,11} This is not surprising, as the underlying chemistry in stain etching and electrochemical etching of Si is recognized to be the same.²⁴ To the best of our knowledge, references 1-16 list all the journal articles published on light-emitting porous Si fabricated by stain etching since Canham's observation of room-temperature luminescence in porous Si in 1990.¹⁸

While numerous papers have appeared on the properties of luminescent porous Si, little has been published on porous Si_{1-x}Ge_x alloys. Gardelis *et al.*¹⁹ report photoluminescence (PL) results for an anodically-etched sample, but only for one alloy composition ($x=0.15$). Because of the variation of band gap with alloy composition, study of the properties of porous Si_{1-x}Ge_x may aid in the understanding the basic mechanism responsible for luminescence in porous Si.

In this paper, the formation of porous Si and Si_{1-x}Ge_x alloys by stain etching and the structural, chemical, and luminescence properties of these layers are reviewed. The implications of these results for the luminescence mechanism is discussed,

2. Production of Porous Silicon and Si_{1-x}Ge_x Alloys by Stain Etching

2.1. Stain Etching of Silicon

Most stain etching of luminescent porous Si has been carried out in HF:HNO₃ based solutions, including HF:HNO₃:H₂O (4:1:5),^{1,8,9,16} HF:HNO₃:H₂O (1:5:10),^{1,13} HF:HNO₃:H₂O (1:3:5),^{4,14,15} HF:HNO₃:CH₃COOH: H₂O (1:2:1:4),³ and HF:HNO₃ (500: 1).¹¹ Stain films have also been produced in NaNO₂:HF (2 g in 100 ml),¹ and CrO₃:HF (0.2 g in 100 ml).¹ In most cases, use of standard electronic-grade reagents has been specified or can be assumed (e.g., 49% HF and 70-71% HNO₃), with the water being deionized. Etching is typically carried out in polypropylene beakers with no intentional heating of the solutions, and etch durations range from 30 sec. to 15 min.

The basic reaction for the etching of Si in HF:HNO₃ based solutions is given as



This oxidation chemistry is the same as that occurring during anodic porosification of Si, with microscopic points on the Si surface behaving randomly as localized anodes and cathodes.²⁴ A more detailed description of the process is given in Ref. 4.

The reaction at the Si surface is **autocatalyzed** by HNO_3 ,²⁴ so that in fresh solutions a quiescent period of several minutes can persist before significant etching occurs. This incubation period in $\text{HF}:\text{HNO}_3:\text{H}_2\text{O}$ (1:3:5) was measured by Steckl *et al.*¹⁴ as a function of **resistivity** (Fig. 1). The incubation time increases with **resistivity** for p-type samples from ≈ 0.5 min. for **0.0043** Q-cm material to ≈ 9 min. for 50 Q-cm material. For n-type material, the incubation time was observed to decrease weakly with increasing resistivity, with times typically of 8-10 min. Shih *et al.*⁴ measured the incubation time as a function of nitric acid content of the solution and found that staining begins almost immediately for nitric content of 40% or greater. In order to accelerate the process in solutions less rich in nitric acid, stain solutions are often **primed**^{1,8} by briefly etching a piece of Si in concentrated $\text{HF}:\text{HNO}_3$ (e.g., 4:1) prior to adding the deionized water. During this process the Si dissolves rapidly, a yellowish gas evolves, and the solution turns yellow. After **diluting** the solution with water, it turns clear again. After priming, the solution contains sufficient HNO_3 that staining of subsequent samples began much sooner.

Gas evolution at the wafer surface can result in bubbles which adhere to the surface and result in **nonuniform** film formation.¹ The appearance of such films to the naked eye is often blackish, with cellular structures ≈ 1 mm in diameter. To avoid bubble formation, the wafers may be dipped in and out of the solution as the films thicken. Bubble formation during etching becomes difficult to avoid for thicker films, so that most of the porous films studied here are 100 to 200 nm in thickness. Note that this is considerably thinner than most **anodically-produced** films discussed in the literature. Shih *et al.*⁴ measured the thickness of porous layers as a function of time elapsed since onset of the stain reaction (Fig. 10). They find that the thickness tends to saturate at about 400 to 600 nm. This is thought to be determined by balancing of the dissolution rates of Si at the porous/bulk interface and the surface of the porous layer.

Electrochemical etching behavior and pore morphology vary considerably depending on Si dopant type and concentration.²⁵ For this reason, several different types of Si wafers were stain etched in $\text{HF}:\text{HNO}_3:\text{H}_2\text{O}$. In solutions rich in HF, etching is expected to be limited by the oxidation process, while in solutions very low in HF, the etching process is expected to be limited by diffusion of the completing fluoride species.²⁶ In order to examine both regimes, etching was carried out in solutions of $\text{HF}:\text{HNO}_3:\text{H}_2\text{O}$ with ratios of 4:1:5 and 1:4:5 by volume. A solution of 1:10:10 was tried as well, but stain films did not nucleate readily. The most controllable and uniform stain film formation occurs for p- wafers using the 4:1:5 solution. These films are specular and exhibit a series of interference colors as the films thicken, such as observed for oxidation of Si. For heavily p-type wafers and for n-type wafers, stain films tended to form in small patches on the wafer surface. All of these stain films exhibit red to orange luminescence to the naked eye under ultraviolet irradiation,

In addition to bulk Si wafers, stain etching has also been carried out on Si on sapphire,¹³ polycrystalline Si on oxidized Si substrates and on quartz,¹⁵ and partially-crystallized amorphous layers on Si substrates.⁷ These experiments demonstrate the relative flexibility of stain etching compared to anodic etching.

2.2. Stain Etching of $\text{Si}_{1-x}\text{Ge}_x$ Alloys

Stain etching of $\text{Si}_{1-x}\text{Ge}_x$ alloy layers has been reported by Ksendzov *et al.*¹⁶ The starting layers were grown by molecular beam epitaxy (MBE) on p-type (100)-oriented Si wafers doped at 1-3 $\Omega\text{-cm}$. The growth was carried out in an MBE system with a base pressure in the low 10-11 Torr range. Si and Ge were coevaporated from separate electron-gun evaporators, with the substrate held at 500-550° C. The $\text{Si}_{1-x}\text{Ge}_x$ layers were doped with boron at 1017-1018 cm^{-3} and were $\approx 0.75\ \mu\text{m}$ thick. Layers with $x < 0.15$ are expected to be below the critical thickness for introduction of misfit dislocations (a consequence of the lattice mismatch between Si and Ge).²⁵ Those layers above the critical thickness are expected to contain a network of misfit dislocations at the $\text{Si}_{1-x}\text{Ge}_x/\text{Si}$ interface and also a high density ($\approx 10^8\ \text{cm}^{-2}$) of threading dislocations running from the interface to the surface of the epitaxial layer. The layers were observed to stain in a manner similar to that observed for Si, with stain films of typical thickness 150 nm. The bulk of the 750 nm alloy layers were not etched, so that the porous regions did not extend into the Si substrates. Preferential attack of threading dislocations was observed in epitaxial layers above the critical thickness, leading to locally thicker stain films, as seen in Fig. 2.

2.3. Selective-area Production of Porous Silicon by Stain Etching

If porous Si devices are to be useful as integrated components of monolithic Si circuitry, selective area production of porous Si will be required. While this may prove difficult in some configurations using anodic etching techniques, it is straight forward with stain etching, and has been demonstrated using a few different approaches.

As noted for $\text{Si}_{1-x}\text{Ge}_x$ alloys, crystallographic defects are recognized to nucleate or enhance the etching procedure. Stain etches can be nucleated selectively by damaging Si through a photoresist or other mask. This has been demonstrated with ion implantation (using unannealed implants), plasma etching, and Ar ion milling.²⁸

Another method used to achieve selective area porosification of Si is selective doping of n-type Si with a Ga^+ focused ion beam. Using this method, photoluminescence patterns with submicron resolution were obtained. A third method employed to realize selective area luminescent porous Si is patterning of polycrystalline Si films on oxidized Si followed by stain etching.¹⁵

2.4. Fabrication of Amorphous/Crystalline Superlattices by Stain Etching

In addition to single porous layers, stain etching has been employed by Fathauer *et al.*⁶ to fabricate superlattices consisting of alternating layers of porous-amorphous $\text{Si}_{1-x}\text{Ge}_x$ alloys and crystalline Si. This is made possible by a high selectivity in the porosification of $\text{Si}_{1-x}\text{Ge}_x$ alloy layers over that of adjacent Si layers in $\text{Si}_{1-x}\text{Ge}_x/\text{Si}$ superlattices grown by MBE. The as-grown superlattices are first ion milled to form mesa structures, followed by immersion in an $\text{HF}:\text{HNO}_3:\text{H}_2\text{O}$ (4:1:4) solution for about 45 sec. The lateral penetration of the pores in the $\text{Si}_{1-x}\text{Ge}_x$ alloy layers without porosification of the adjacent Si layers is approximately $0.75\ \mu\text{m}$, so that $1\ \mu\text{m}$ wide mesas can be fully converted to porous/non-porous superlattices. porous layers as thin as

5 nm have been demonstrated by this technique. Transmission electron microscopy and diffraction characterization of these structures shows the porous alloy layers to be amorphous, so that a unique amorphous/crystalline superlattice structure is obtained (Fig. 3).

3. Microstructural Properties

3.1. *Surface and Interface Morphology*

The surface morphology of stain-etched porous Si has been studied with scanning electron microscopy (SEM)^{1,4,13,14,15} and atomic force microscopy (AFM),^{3,5} while the interface between stain-etched porous Si and the Si substrate has been studied with transmission electron microscopy (TEM).^{1,5}

In contrast to electrochemically-etched porous Si, relatively little variation with wafer type in the structure of the films is seen. The microstructure is difficult to observe by SEM, unless bubble formation is allowed during etching (Fig. 4).¹ The surface is more easily imaged using AFM (Fig. 5), where a smooth surface with large dips is observed. Anodically etched films show more fine-scale bumpiness.⁵

Stain films produced from $\text{Si}_{1-x}\text{Ge}_x$ alloys appear relatively featureless in the SEM for samples where the alloy layer is below critical thickness. Above critical thickness, however, a high density of pits is observed. This is due to preferential attack along threading dislocations, as seen in Fig. 2. Rough morphology is also noted in porous Si-on-sapphire wafers,¹³ presumably for the same reason.

While porous Si layers produced by stain etching appear extremely uniform throughout their depth in TEM cross sections (see below), the interface between the porous layer and the unetched Si substrate is rough, exhibiting a feathery appearance (Fig. 6).¹

3.2. *Crystallinity*

The bulk structure and crystallinity of stain-etched porous Si has been studied with TEM,^{1,5,12} transmission electron diffraction (TED),^{5,12} and reflection high-energy electron diffraction (RHEED).³⁰

TEM analyses have been performed in three very distinct manners: using conventional cross-sectional specimen preparation techniques,^{1,5} simple cleaving of samples for examination in cross section,⁵ and preparation of a plan-view TEM specimen from bulk Si followed by stain etching of the TEM specimen.¹² Conventional preparation has been suggested to possibly damage the layers,³¹ as it involves the use of solvents as well as ion-beam thinning. This damage is not expected to completely amorphize porous layers, however. The cleavage technique involves no solvents, and no heat treatments as a room temperature epoxy is used. There is limited viewable area, however, as only the tip of the cleaved wedge is electron transparent. This technique also has a distinct advantage over the scraping technique employed by Cullis and Canham³¹ in that the layer remains intact so that information such as the depth within the porous layer is preserved. Finally, the staining of a prepared TEM specimen is another scheme for

avoiding exposure to post-stain-etching treatments. It has the disadvantage that the starting Si has been exposed to conventional specimen preparation procedures and therefore may not etch in the same manner as a virgin Si wafer.

Some stain-etched porous Si films examined in cross-section appear completely amorphous, whether conventional or cleavage techniques were used.⁵ An example of TEM and TED data from a cleaved specimen is shown in Fig. 7. Amorphous as well as partially crystalline regions were observed in the plan-view specimens described above.¹² In some conventionally-prepared cross sections, crystallite are observed with diameters in the range of 1-3 nm. These are observed in Si_{1-x}Ge_x alloy layers as well (Fig. 8). The density of these crystallite is highest near the interface with the unetched region, with few or no crystallite observed near the surface. No difference was noted in the PL of samples which contained small crystallite and those which were fully amorphous.

RHEED data were obtained by Fathauer et al.³⁰ on full two-inch wafers etched in three different stain solutions: HF:HNO₃:H₂O, NaNO₂:HF, and CrO₃:HF. The samples were immediately loaded into a nitrogen-purged glove box attached to the load lock of an MBE system. The wafers were placed on a spinner and briefly etched in an HF:ethanol solution to remove any surface oxide which would obscure the diffraction pattern from the porous Si. The samples were then loaded directly into the MBE system, the load lock of which is attached to the glove box. A 10-kV electron beam was directed at the wafer surfaces at grazing incidence, with the resulting diffraction pattern displayed on a phosphor screen. No sign of crystallinity was observed for any azimuth for the luminescent HF:HNO₃:H₂O or NaNO₂:HF films. On the other hand, a spot pattern indicative of transmission of the electron beam through small crystalline features was observed for the CrO₃:HF-etched sample, which did not show any PL.

3.3. Porosity

While the porosity of porous Si has most commonly been measured by gravimetric analysis, this is not possible for the stain-etch case, where the thickness of the porous film is only a small fraction of the total wafer thickness. For this reason, Pike et al.²⁹ employed energy-dispersive x-ray spectroscopy (EDX) of a TEM cross section to profile the porosity of porous Si and Si_{1-x}Ge_x layers at the nanometer level. By comparing the x-ray counts produced in the porous region to those produced in the bulk region, the porosities in the near surface region are shown to be between 70 and 80% for both Si and Si_{1-x}Ge_x layers.

4. Composition and Chemical Properties

Characterization of the chemical bonding and elemental composition of stain-etched films has been carried out with x-ray photoelectron spectroscopy (XPS),² Rutherford backscattering spectroscopy (RBS),^{16,32} elastic recoil detection (ERD),³² parallel electron-energy loss spectroscopy (PEELS),²⁹ EDX,²⁹ and electron spin resonance (ESR).³³

4.1. Elemental Composition

Both porous Si and $\text{Si}_{0.7}\text{Ge}_{0.3}$ alloys have been characterized with RBS to determine C levels, with ERD to determine H levels, and $\text{Si}_{1-x}\text{Ge}_x$ alloys with EDX for profiling of the alloy content as a function of depth in the porous layer. The estimated composition of porous Si from RBS and ERD analyses, made approximately one day after stain etching, is $\text{Si}_{0.73}\text{C}_{0.02}\text{H}_{0.25}$ (oxygen below detection limit of $\approx 1\%$). The $\text{Si}_{0.7}\text{Ge}_{0.3}$ sample showed comparable C and H levels but also 1-2% O.³² XPS survey scans of porous Si layers rinsed with an HF:ethanol solution just prior to examination show trace amounts of O, C, and Fe in a predominantly Si matrix.²

Examination of $\text{Si}_{1-x}\text{Ge}_x$ layers with XPS before and after stain etching indicates a marked increase in the percentage of Ge in the material after porosification.¹⁶ RBS analysis also shows this effect,¹⁶ The Ge concentration in porous alloy layers has been profiled as a function of depth by Pike *et al.* using PEELS.²⁹ The Ge:Si ratio is highest near the surface, decreasing as the porous/bulk interface is approached. The porosity profile obtained with EDX is observed to follow a similar trend.

4.2. Electronic Structure and Chemical Bonding

The Si bonding in the near-surface region of porous Si formed by stain etching has been examined by Vasquez *et al.*² by performing Si 2p and valence-band XPS measurements. This was carried out for films stained in HF:HNO₃:H₂O, NaNO₂:HF, and CrO₃:HF. Both the luminescent HF:HNO₃:H₂O and NaNO₂:HF etched films show spectra characteristic of amorphous Si. On the other hand, the non-luminescent CrO₃:HF etched film shows structure characteristic of crystalline Si, though of poor quality.

George *et al.*³³ have carried out ESR measurements on stain etched porous Si. A resonance is observed at a g value of 2.0056 ± 0.0002 , with a linewidth of ≈ 6.25 G at room temperature. This resonance, which is absent in a reference bulk Si sample, coincides with the resonance ascribed in the literature to single Si dangling bonds in amorphous Si. The approximate number of spin centers contributing to the resonance line width suggest that the layer consists predominantly of amorphous rather than crystalline Si.

5. Luminescence Properties

A number of groups have performed PL characterization of stain-etched Si,¹⁻¹⁶ and PL of stain-etched $\text{Si}_{1-x}\text{Ge}_x$ alloys with a wide range of x has been carried out as well.¹⁶ While there is considerable literature on the PL properties of anodically-etched porous Si, there is very little on $\text{Si}_{1-x}\text{Ge}_x$ alloys, so that detailed comparison of stain-etch and anodic-etch results is not possible. To date, only one group has reported results on electroluminescent (EL) diodes fabricated from stain-etched Si.¹⁰

5.1. Photoluminescence

Both Kidder *et al.*⁹ and Aoyagi *et al.*¹¹ have carried out detailed comparisons of the luminescence properties of stain-etched and anodically-etched Si. Aoyagi *et al.* have measured excitation and luminescence spectra and find that stain-etched and anodically-etched films both contain virtually the same luminescence band around 595 nm and the

same excitation band (i.e., absorption band) around 263 nm. Based on these results they conclude that the two types of porous Si contain similar luminous material.

Kidder *et al.* examined stain-etched films produced in solutions with a wide range of $\text{HF}:\text{HNO}_3:\text{H}_2\text{O}$ ratios. The peak position of the PL spectra was found to lie at ≈ 650 nm for all layers. Stain-etched films soaked in 10% HF (by volume) for between 10 and 60 min. showed no significant change in PL peak position. For anodically-etched films, on the other hand, they found PL peak positions varying from 640 nm to 710 nm, depending on the electrolyte HF concentration. The luminescence of the stain-etched films was thus found to exhibit less dependence on process conditions than that of anodically-etched films. The PL intensity of stain-etched Si was found to decrease exponentially under room-temperature illumination at 476 nm, with a time constant of ≈ 22 min. (Fig. 9). They found less severe degradation of the PL magnitude in anodically-etched films.

All of the authors cited in Refs. 1-16 report similar PL spectra for stain-etched Si except for Belov.¹⁰ In this case, three narrow peaks centered at 760, 768, and 785 nm were observed, rather than the single broad peak observed by other authors. Since no structural characterization of these films is presented, it is not certain that they are actually similar to porous films reported elsewhere. The etching procedure employed and appearance of the film to the naked eye are consistent with other reports for stain films, however.

The peak intensity of the PL from stain-etched films is reported to be lower than that of anodically-etched films by a factor of 3-10.^{4,11,30} Because stain films are usually much thinner than anodic films, this could well be due simply to the presence of less volume of material to excite luminescence from. A decay in the luminescence intensity upon annealing in vacuum has been observed by Sarathy *et al.*³ which is similar to that observed by several groups for anodically-etched Si. The luminescence drops rapidly around 400°C, and was found to be partially recoverable through HF dipping.

Photoluminescence spectra have also been reported for stain-etched Si on sapphire¹³ and for polycrystalline Si films.¹⁵ In both cases, the PL spectra are similar to those obtained for stain-etched bulk Si wafers. Amorphous Si films subjected to stain etches have been reported not to luminesce.¹⁵

Luminescence data for $\text{Si}_{1-x}\text{Ge}_x$ alloys of various x have been reported by Ksendzov *et al.*¹⁶ The Ge content of the layers, as noted above, was found to increase upon stain etching. Data for x before (after) etching of 0.04 (0.06), 0.07 (≈ 0.15), 0.11 (0.23), 0.15 (≈ 0.5), 0.20 (0.88), 0.30 (not measured), and 0.40 (not measured) were obtained. Bulk Ge was also etched and found not to luminesce. Photoluminescence intensity is found to decrease dramatically with increasing Ge content, as shown in Fig. 11. For a porous film formed from a layer with $x = 0.3$, the PL intensity is orders of magnitude lower than that of porous Si. There is no consistent and significant shift in the peak position, however, in spite of a considerable change in band gap of the bulk alloys with Ge content.

5.2. Electroluminescence

The only report of EL from stain-etched Si to date is by Belov.¹⁰ As noted above, the PL reported for these films is quite different from that reported by other authors, so that it is not clear if these films are actually similar in nature to the porous Si films formed by other authors. Diodes were fabricated by metallizing the backside of a p-type (1 11) wafer of 10 $\Omega\text{-cm}$ resistivity, followed by protection of the backside with laquer and immersion in a 40% aqueous solution of HF with a small amount of nitric acid for 30-45 s. A semitransparent layer of Al or Au was then deposited through a mask. Under forward bias, stable emission was first noted at 1.4 V, with a corresponding current density of 100 mA/cm^2 . Increasing the current density by a factor of 800 increased the intensity of emission by three orders of magnitude. The EL spectrum at a current density of 60 A/cm^2 is peaked at around 580 nm and is comparable in spectral width to typical PL spectra of porous Si.

6. Implications for Mechanism of Luminescence

Two major pieces of information have come out of work on stain-etched porous Si which have significant implications for the luminescence mechanism in all Si. The first of these is the fact that stain-etched layers appear to be predominantly or completely amorphous, yet exhibit PL that is virtually identical to that of anodically-etched layers. The second is the PL data for a comprehensive set of $\text{Si}_{1-x}\text{Ge}_x$ alloy layers, showing no significant shift in peak PL wavelength with alloy composition, along with a dramatic decrease in the peak intensity. It should be possible to obtain the same sort of alloy data with anodic etching, but such data does not appear to be extant in the literature. Since it is unlikely that different mechanisms are responsible for the very similar luminescence in stain-etched and anodically-etched Si, the implications of these results for the luminescence mechanism in stain-etched Si apply to all porous Si.

6.1. Amorphous Nature of Porous Silicon Produced by Stain Etching

While porous Si layers etched by anodic techniques generally consist of a mixture of crystalline and amorphous material,⁴² and are often predominantly crystalline, stain-etched Si is predominantly or completely amorphous. The following techniques have been used to verify the amorphous nature of stain-etched Si: TEM lattice imaging, TED, RHEED, XPS, and ESR. In some films, a low density of crystallite is observed near the porous/bulk interface, but these are present in insufficiently large quantity to account for the relatively bright luminescence observed.

Note that the different techniques used to verify the amorphous nature actually measure quite different quantities. TEM and TED are sensitive to crystallinity with at least short range order (a few atomic spacings) in the bulk of the porous layer. RHEED probes crystallinity on a similar scale, but only in the top ≈ 10 nm of the layer. XPS is primarily sensitive to nearest-neighbor and next-nearest-neighbor bonds. ESR is also sensitive to nearest neighbor bonding. The fact that all of these techniques fail to reveal crystallinity is strong evidence against crystalline quantum wires or dots in the usual sense; i.e., a structure with a well-defined lattice (diamond cubic or other) and dimensions of ≈ 2 -10 nm.

This result does not necessarily imply that amorphous Si itself is the luminescing species, but is consistent with any molecular unit or structure too small to actually form a regular three-dimensional lattice. This includes siloxene,³⁸ organic contaminants trapped in the porous material,⁴⁰ and the sort of two-dimensional lattices proposed by Van de Walle.⁴¹

The mechanism by which initially crystalline Si becomes amorphous upon stain etching is not known at this time. One possibility is redeposition of Si from solution, but results on Si_{1-x}Ge_x single-layer and superlattice samples suggest this is probably not the mechanism, as the Si_{1-x}Ge_x material appears to stay in place during porosification. Another possibility is a spontaneous phase transformation from crystalline to amorphous material as the dimensions of the Si filaments or particles become very small. Thermodynamic arguments for such a transformation are put forth by Veprek *et al.*,³⁹ who observed x-ray data showing that deposited Si particles below ≈ 3 nm in diameter are amorphous. Similar observations have been reported for Si and Si_{1-x}Ge_x alloys subjected to ball milling.⁴³

6.2. Luminescence behavior of Si_{1-x}Ge_x Alloys

As seen in Fig. 11, the PL peak position shows no significant trend with the Ge content x . According to models of PL due to quantum-size effects (e.g., ref. 34), assuming constant distribution of particle sizes in the various porous layers, the PL peak position is expected to follow the bandgap of the bulk material. For the Ge contents measured for these samples, the peak should monotonically decrease by ≈ 200 meV through this series of samples.¹¹ The possibility of a reduction in average particle size with increasing Ge content is just such a way as to counteract this shift cannot be ruled out, but is unlikely. In addition, under a quantum-size model, the PL peak intensity is not expected to drop with increasing Ge content,

The further argument is made in ref. 11 that one can deduce the size of luminescing clusters under the assumption that a single Ge atom in a cluster quenches the luminescence. Then, using probability theory to fit the rate of decline in the PL intensity, an average cluster of a size containing 7 Si atoms is arrived at. While this is consistent with luminescence originating from small molecular clusters, it is not consistent with quantum dots of wires, where individual particles would contain ≈ 1000 atoms.

7. Conclusions

Most work to date on porous Si has been carried out with anodically-etched films. Stain-etched films have been shown to exhibit very similar luminescence and have the advantage of greater flexibility in the etching process. On the whole, these layers appear to be less crystalline than anodically-etched layers, and are often completely amorphous. In addition to large-area stain-etched porous Si films on bulk wafers, porous-Si on sapphire, porous polycrystalline Si, and selective-area porous Si have all been produced by stain etching. A wide range of epitaxial Si_{1-x}Ge_x alloy layers have been porosified as well. Both the amorphous nature of stain-etched porous Si and the lack of a shift in the

PL peak position in porous $\text{Si}_{1-x}\text{Ge}_x$ alloys provide compelling evidence against quantum-sized crystallite being responsible for the visible luminescence in porous Si.

Acknowledgements

I would like to thank several collaborators for their contributions to this work, including Thomas George, Alex Ksendzov, Richard P. Vasquez, Barry Wilkins, Eric W. Jones, W. Thomas Pike, Anthony P. Taylor, S.S. Kim, and Mark S. Anderson. Work carried out at JPL was performed at the Center for Space Microelectronics Technology, Jet Propulsion Technology, California Institute of Technology, and was sponsored by the Ballistic Missile Defense Organization/Innovative Science and Technology Office, through an agreement with the National Aeronautics and Space Administration.

References

1. R.W. Fathauer, T. George, A. Ksendzov, and R.P. Vasquez, *Appl. Phys. Lett.* **60** (1992) 995.
2. R.P. Vasquez, R.W. Fathauer, T. George, A. Ksendzov, and T.L. Lin, *Appl. Phys. Lett.* **60** (1992) 1004.
3. J. Sarathy, S. Shih, K. Jung, C. Tsai, K.-H. Li, D.-L. Kwong, J.C. Campbell, S.-L. Yau and A.J. Bard, *Appl. Phys. Lett.* **60** (1992) 1532.
4. S. Shih, K.H. Jung, T.Y. Hsieh, J. Sarathy, J.C. Campbell, and D.L. Kwong, *Appl. Phys. Lett.* **60** (1992) 1863.
5. T. George, M.S. Anderson, W.T. Pike, T.L. Lin, R.W. Fathauer, K.H. Jung, and D.L. Kwong, *Appl. Phys. Lett.* **60** (1992) 2359.
6. R.W. Fathauer, T. George, E.W. Jones, W.T. Pike, A. Ksendzov, and R.P. Vasquez, *Appl. Phys. Lett.* **61** (1992) 2350.
7. K.H. Jung, S. Shih, D.L. Kwong, C.C. Cho, and B.E. Gnade, *Appl. Phys. Lett.* **61** (1992) 2467.
8. T.P. Pearsall, J.C. Adams, J.N. Kidder, Jr., P.S. Williams, S.A. Chambers, J. Lath, D.T. Schwartz, and B.Z. Nosho, *Thin Solid Films* **222** (1992) 200.
9. J.N. Kidder, Jr., P.S. Williams, T.P. Pearsall, D.T. Schwartz, and B.Z. Nosho, *Appl. Phys. Lett.* **61** (1992) 2896.
10. S.V. Belov, *Sov. Tech. Phys. Lett.* **18** (1992) 800.
11. H. Aoyagi, A. Motohashi, A. Kinoshita, T. Aono, and A. Satou, *Jpn. J. Appl. Phys.* **32** (1993) L1.
12. S. Shih, K.H. Jung, R.-Z. Qian, and D.L. Kwong, *Appl. Phys. Lett.* **62** (1993) 467.
13. W.B. Dubbelday, D.M. Szaflarski, R.L. Shimabukuro, S.D. Russell, and M.J. Sailor, *Appl. Phys. Lett.* **62** (1993) 1694.
14. A.J. Steckl, J. Xu, H.C. Mogul, and S. Mogren, *Appl. Phys. Lett.* **62** (1993) 1982.
15. A.J. Steckl, J. Xu, and H.C. Mogul, *Appl. Phys. Lett.* **62** (1993) 2111.
16. A. Ksendzov, R.W. Fathauer, T. George, W.T. Pike, R.P. Vasquez, and A.P. Taylor, *Appl. Phys. Lett.* **63** (1993) 200.
17. A. Uhler, *Bell System Tech. J.* **35** (1956) 333.
18. L.T. Canham, *Appl. Phys. Lett.* **57** (1990) 1046.
19. S. Gardelis, J.S. Rimmer, P. Dawson, B. Hamilton, R.A. Kubiak, T.E. Whall, and E.H.C. Parker, *Appl. Phys. Lett.* **59** (1991) 2118.
20. T.P. Pearsall, J.C. Adams, J.E. Wu, B.Z. Nosho, C. Aw, and J.C. Patton, *J. Appl. Phys.* **71** (1992) 4470.
21. M.W. Cole, J.F. Harvey, R.A. Lux, D.W. Eckart, and R. Tsu, *Appl. Phys. Lett.* **60** (1992) 2800.
22. P.C. Searson, J.M. Macaulay, and F.M. Ross, *J. Appl. Phys.* **72** (1992) 253.
23. R.J. Archer, *J. Phys. Chem. Solids* **14** (1960) 104.
24. Sorab K. Ghandi, *VLSI Fabrication Principles* (Wiley, New York, 1983), pp. 478-482.

25. J.C. Bean, in *Silicon Molecular Beam Epitaxy*, Vol. II, ed. by E. Kasper and J.C. Bean (CRC Press, Boca Raton, 1988), pp. 65-110.
26. B. Schwartz and H. Robbins, *J. Electrochem. Soc.* 123 (1976) 1903.
27. M.I.J. Beale, J.D. Benjamin, M.J. Uren, N.G. Chew, and A.G. Cullis, *J. Crystal Growth* 75 (1986) 408.
28. R.W. Fathauer, T. George, E.W. Jones, A. Ksendzov, T.L. Lin, W.T. Pike, and R.P. Vasquez, presented at the 1991 Fall Meeting of the Materials Research Society (Boston, MA, December 2-6, 1991).
29. W.T. Pike, A. Ksendzov, R.W. Fathauer, and T. George, *J. Vat. Sci. Technol* (to be published).
30. R.W. Fathauer, T. George, A. Ksendzov, T.L. Lin, W.T. Pike, R.P. Vasquez, and Z.-C. Wu, in *Mat. Res. Soc. Symp. Proc.*, Vol. 256, ed. by S.S. Iyer, R.T. Collins, and L.T. Canham (Materials Research Society, Pittsburgh, 1992), pp. 165-168.
31. A.G. Cullis and L.T. Canham, *Nature* 353 (1991) 335.
32. R.W. Fathauer and B. Wilkins (unpublished).
33. T. George, R.P. Vasquez, S.S. Kim, R.W. Fathauer, and W.T. Pike, in *Mat. Res. Soc. Symp. Proc.*, Vol. 259, ed. by R.J. Nemanich, C.R. Helms, M. Hirose, and G.W. Rubloff (Materials Research Society, Pittsburgh, 1992), pp. 415-420.
34. M. Voos, Ph. Uzan, G. Bastard, and A. Halimaoui, *Appl. Phys. Lett.* 61 (1992) 1213.
35. R.W. Fathauer et al. JVST (to be published).
36. R.W. Fathauer, unpublished.
37. D.R. Turner, *J. Electrochem. Soc.* 107, (1960) 810.
38. M.S. Brandt, H.D. Fuchs, M. Stutzman, J. Weber, and M. Cardona, *Solid State Communications* 81 (1992) 307.
39. S. Veprek, Z. Iqbal, and F.A. Sarott, *Phil. Mag. B* 45 (1982) 137.
40. B.A. Wilson, *Phys. Rev. B* 23 (1981) 3102,
41. C.G. Van de Wane and J.E. Northrup ??? (1993).
42. C. Pickering, M.I.J. Beale, D.J. Robbins, P.J. Pearson, and R. Greef, *J. Phys. C: Solid State Phys.* 17 (1984) 6535.
43. E. Gaffet, F. Faudot, and M. Harmelin, *Mat. Sci. and Eng.* A149 (1991) 85.

Fig. 1. Incubation time for staining of Si as a function of n- and p-type wafer resistivity (from Steckl *et al.* in ref. 14).

Fig. 2. TEM cross section of a stained 0.75- μm -thick $\text{Si}_{0.7}\text{Ge}_{0.3}$ layer (from Fathauer *et al.* in ref. 35).

Fig. 3. TEM cross section of amorphous/crystalline superlattice formed by stain etching of an epitaxial $\text{Si}/\text{Si}_{0.7}\text{Ge}_{0.3}$ superlattice grown by MBE (from Fathauer *et al.* in ref. 6).

Fig. 4. SEM micrographs of stain etched Si produced by (a) etching 0.05 $\Omega\text{-cm}$ B-doped Si(100) in 1:5:10 $\text{HF}:\text{HNO}_3:\text{H}_2\text{O}$ (bubbles allowed to form on wafer surface) and (b) etching 1-3 $\Omega\text{-cm}$ B-doped Si(100) in 4:1:5 $\text{HF}:\text{HNO}_3:\text{H}_2\text{O}$ (bubbles not allowed to form (from Fathauer *et al.* in ref. 1).

Fig. 5. AFM profile image of stain etched Si (from George *et al.* in ref. 5).

Fig. 6. Cross-sectional TEM micrographs of (a) a film produced by etching 0.05 $\Omega\text{-cm}$ B-doped Si(100) in 1:5:10 $\text{HF}:\text{HNO}_3:\text{H}_2\text{O}$ and (b) a film produced by etching 1-3 $\Omega\text{-cm}$ B-doped Si(100) in 4:1:5 $\text{HF}:\text{HNO}_3:\text{H}_2\text{O}$. (c) Diffraction pattern from the thick layer of Fig. 6b, showing the material to be amorphous. The sample shown in 6a evolved gas rapidly during etching, while no surface bubbles were observed in the etching of the sample shown in 6b. The dark contrast at the bottom of the void in Fig. 6a is likely due to deposition of Cr (for preservation of the surface during specimen preparation) through the hole at the top of the void. Both micrographs are at the same magnification (from Fathauer *et al.* in ref. 1).

Fig. 7. Cross-sectional TEM micrograph of a wedge specimen prepared from stain-etched Si (from George *et al.* in ref. 5).

Fig. 8. TEM cross section of a stain-etched $\text{Si}_{1-x}\text{Ge}_x$ alloy layer showing nanocrystals near the porous/bulk interface (from Pike *et al.* in ref. 29).

Fig. 9. Degradation of room temperature photoluminescence from stain-etched Si under illumination at 476 nm in air. Excitation optical power was 15 mW (chopped with 30 mW beam). Inset shows log intensity vs. illumination time indicating a simple decay process where the intensity decreases by $1/e$ over 22.45 min. (from Kidder *et al.* in ref. 9).

Fig. 10. Variation of porous film thickness of p-type 6-7 $\Omega\text{-cm}$ Si after stain etching in 1:3:5 $\text{HF}:\text{HNO}_3:\text{H}_2\text{O}$ with reaction time for two different stirring conditions (from Shih *et al.* in ref. 4).

Fig. 11. PL of stain-etched $\text{Si}_{1-x}\text{Ge}_x$ alloy layers (from Ksendzov *et al.* in ref. 16).

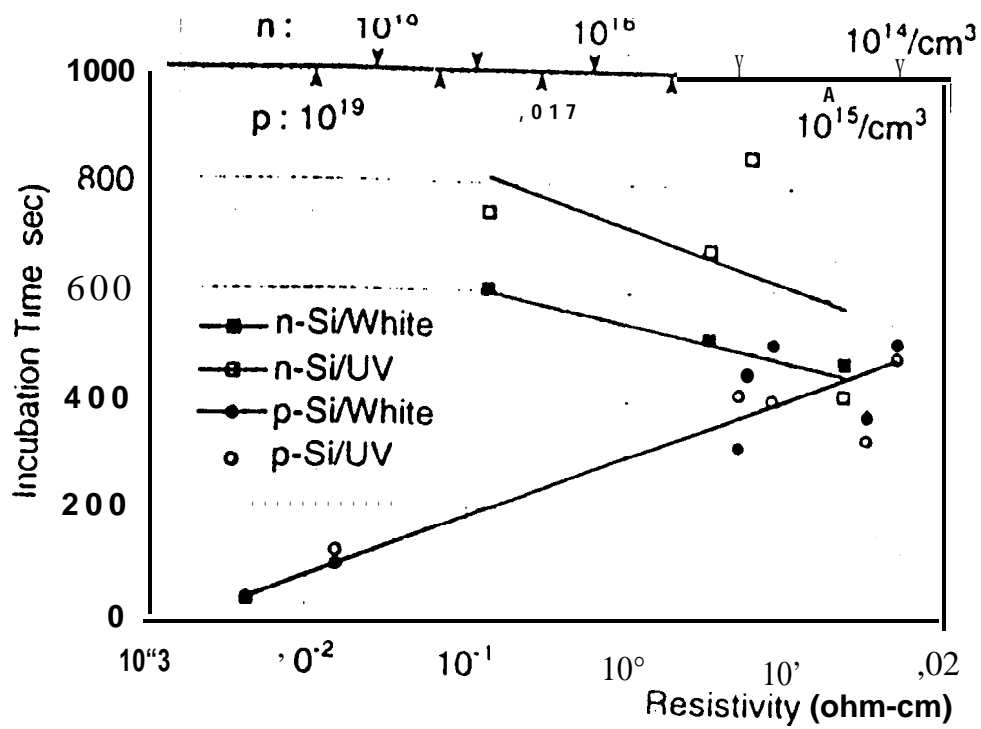


Fig. 1

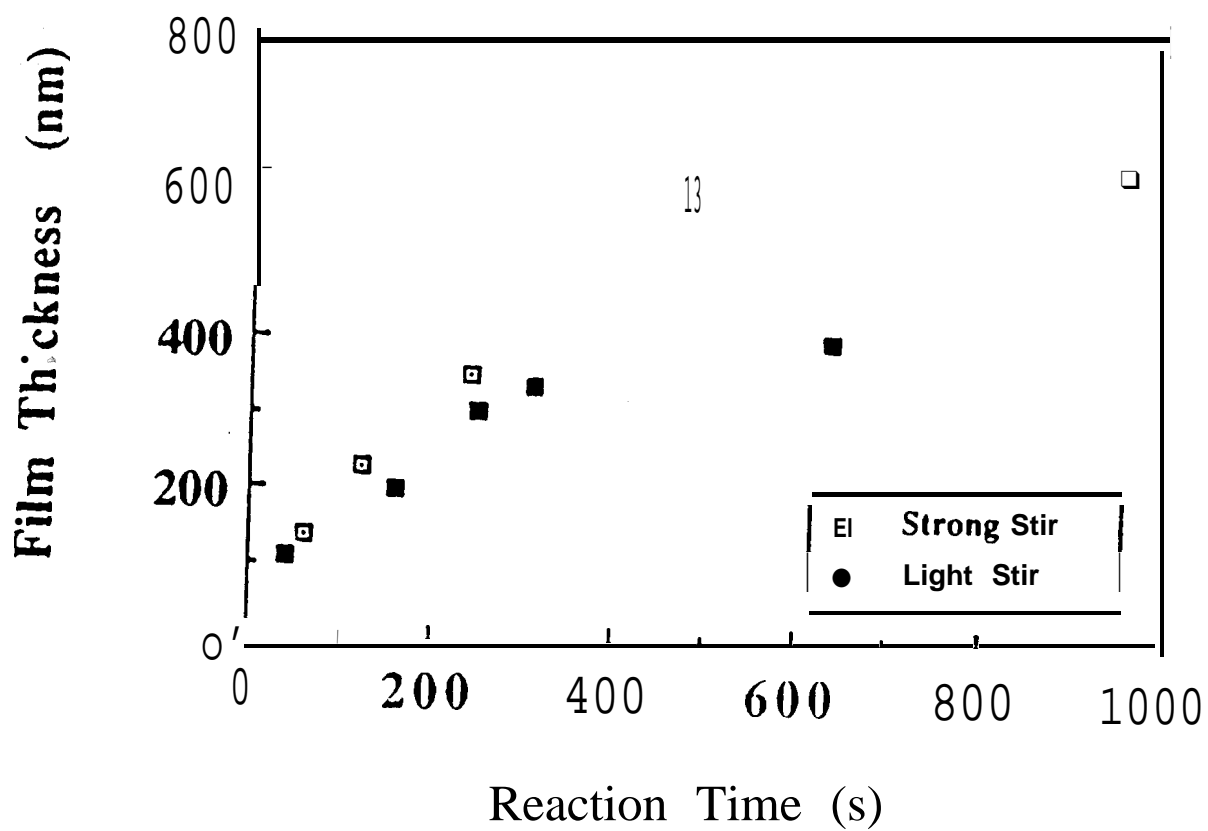
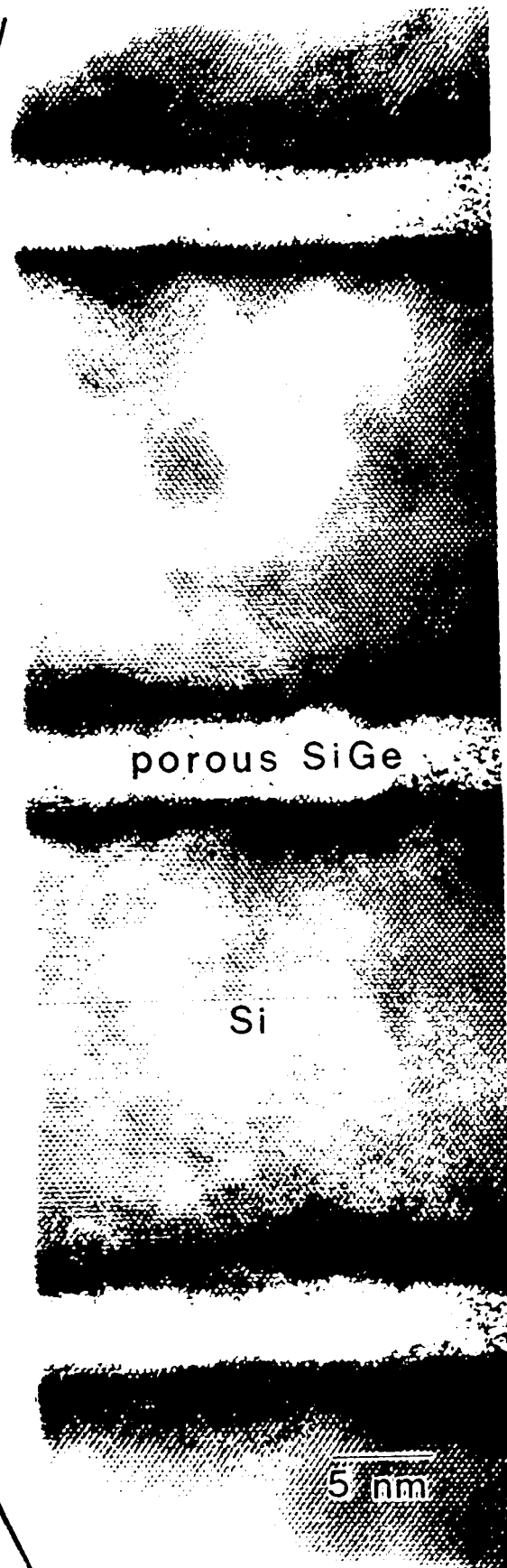


Fig. 10

REF ID: A66





Transmission electron micrograph of the porous SiGe/Si heterostructure. The lattice spacing of the Si layer is indicated by the arrow.

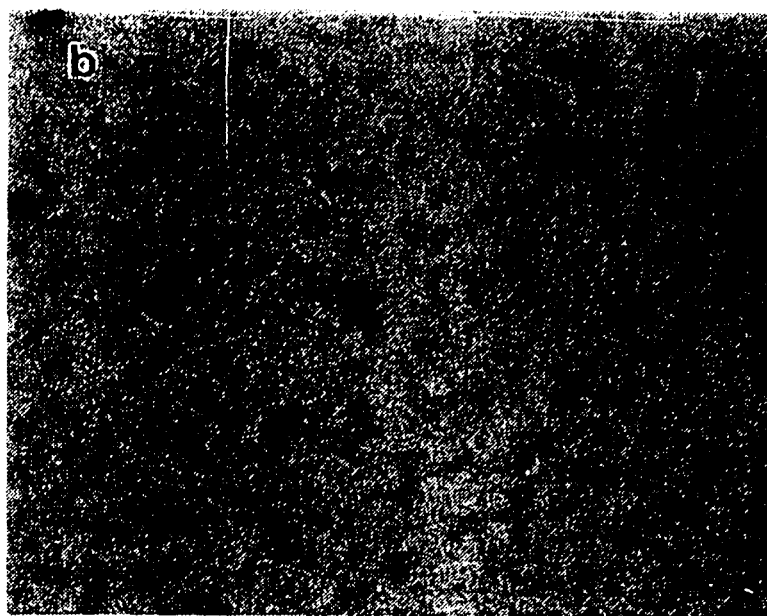
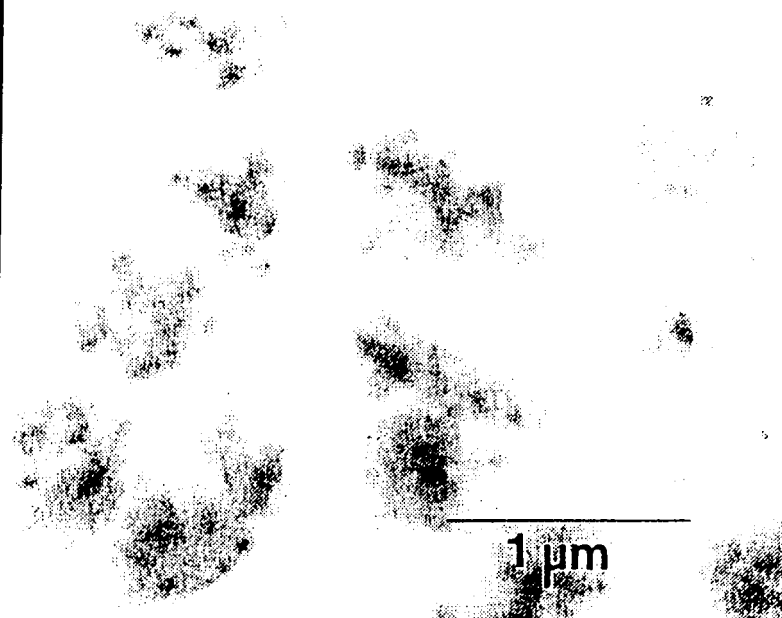
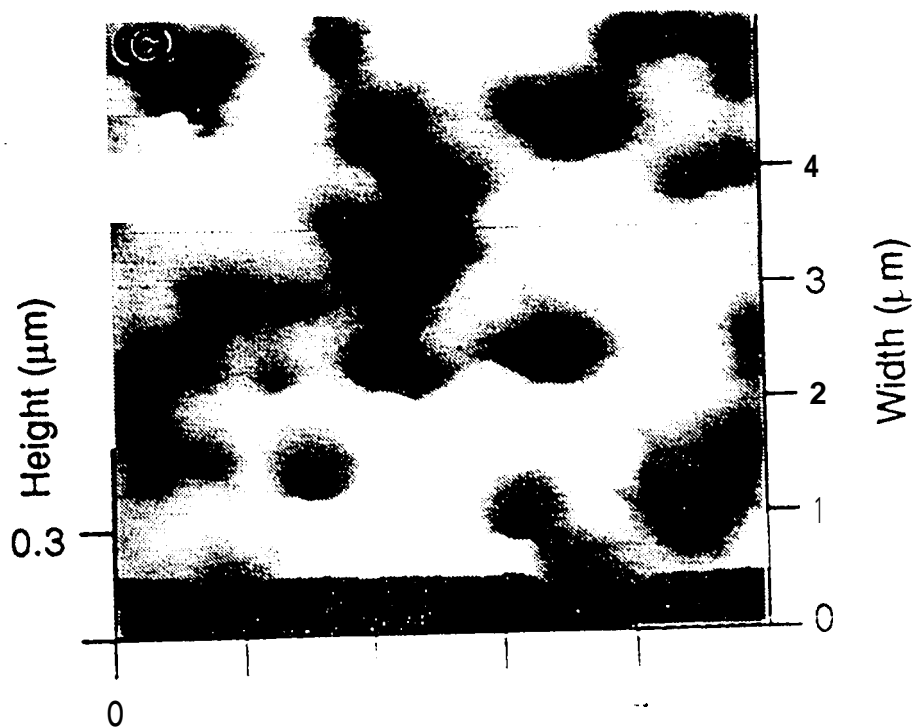


Fig. 4



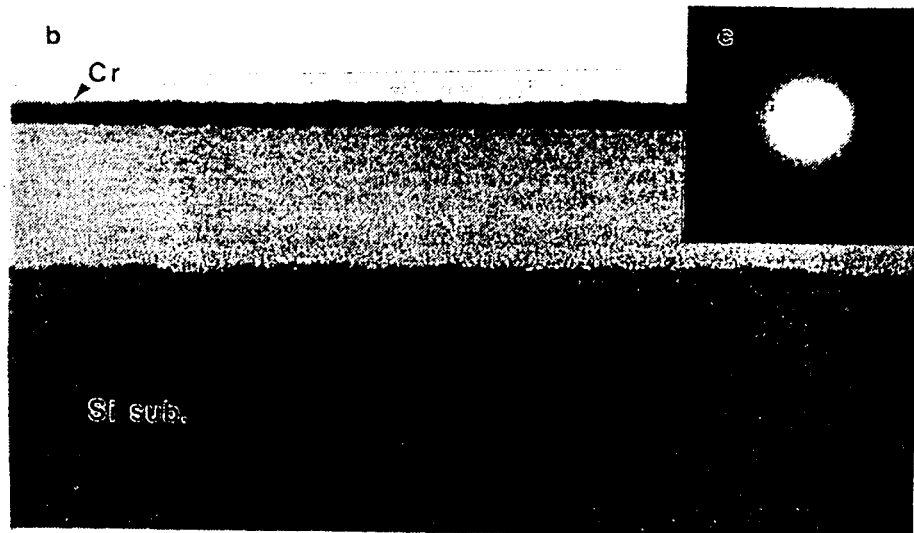
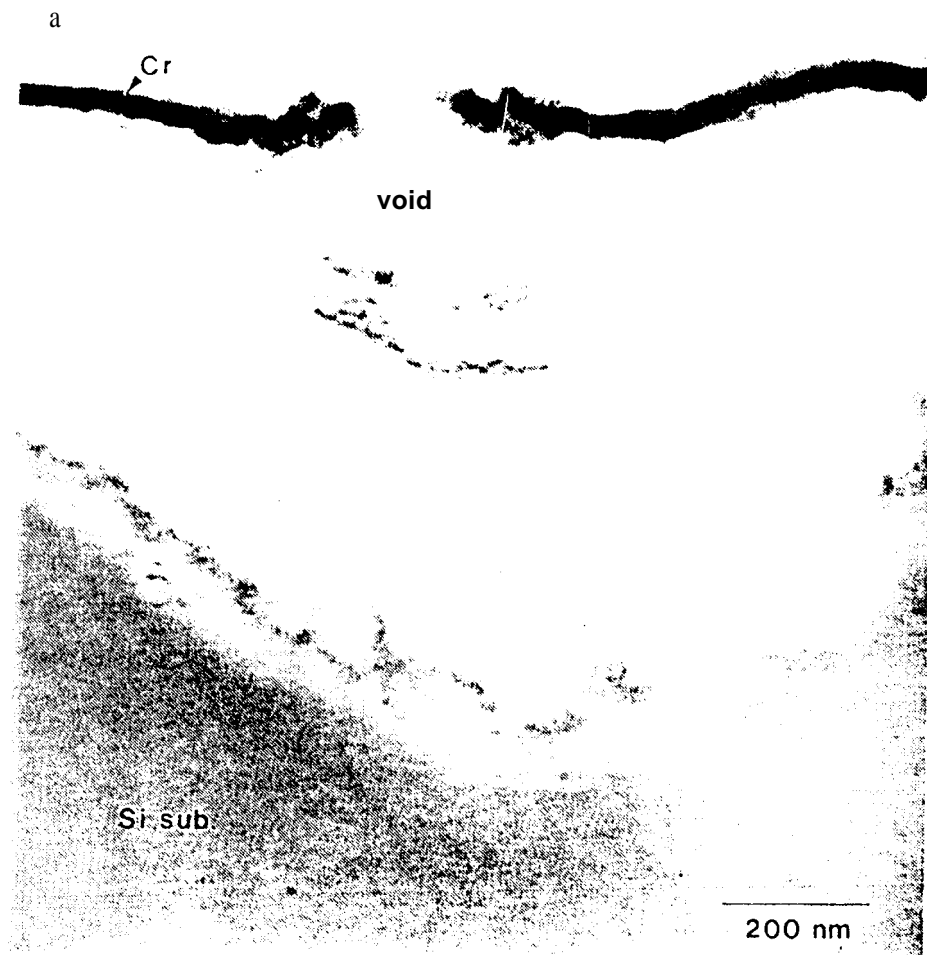


Fig 6

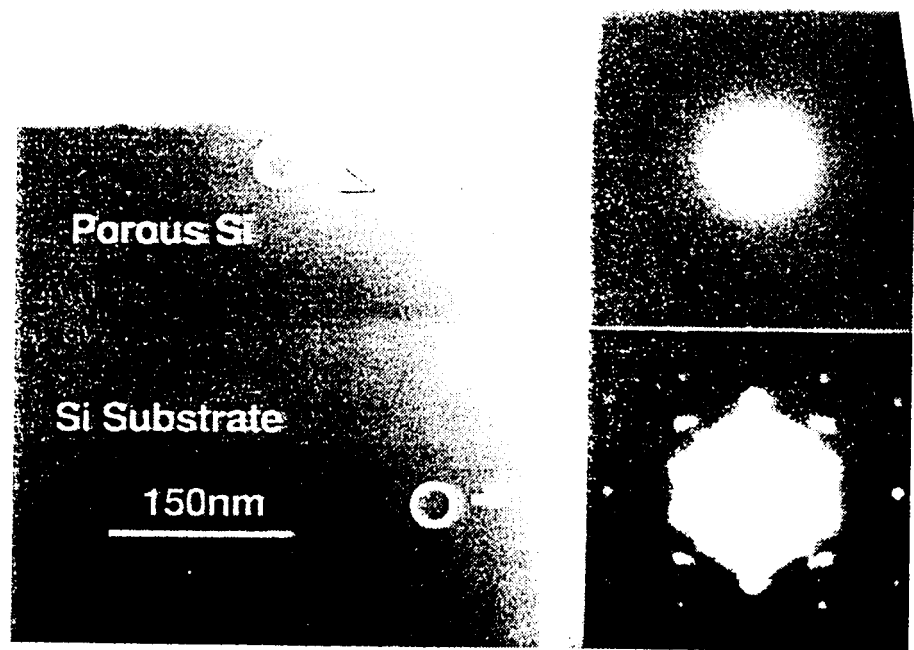


Fig. 7



10nm

Fig 8

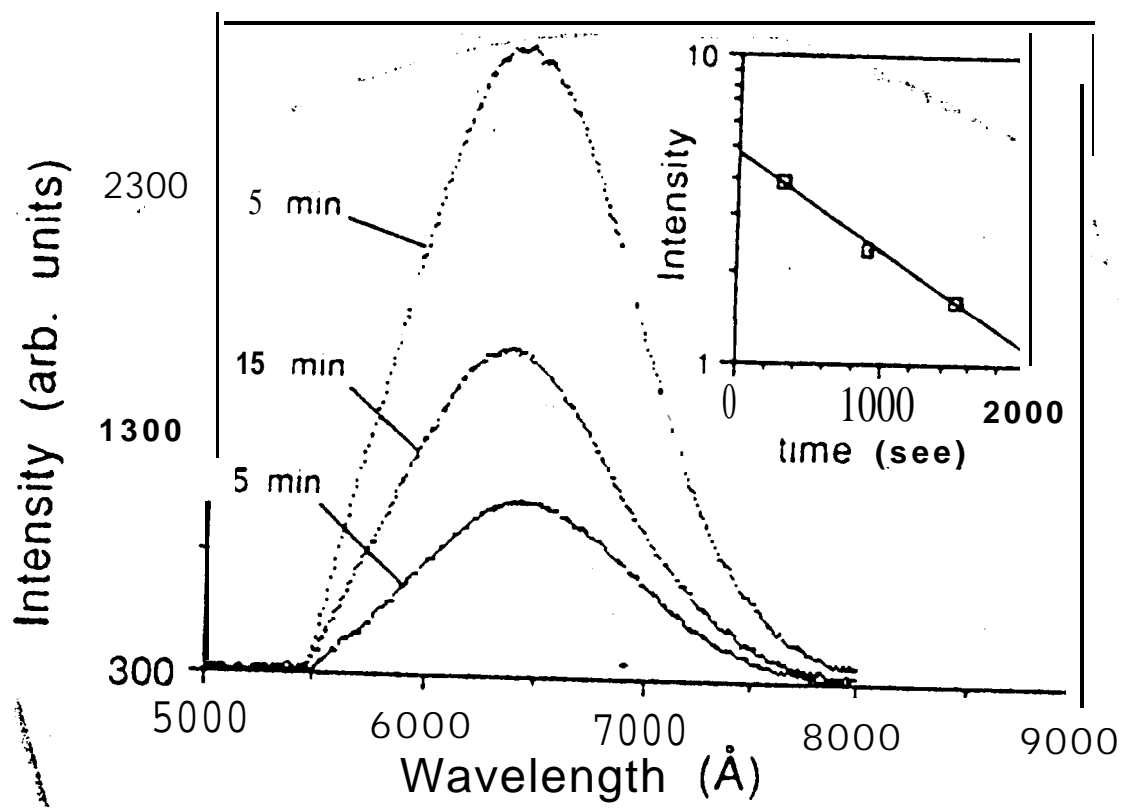


Fig. 9

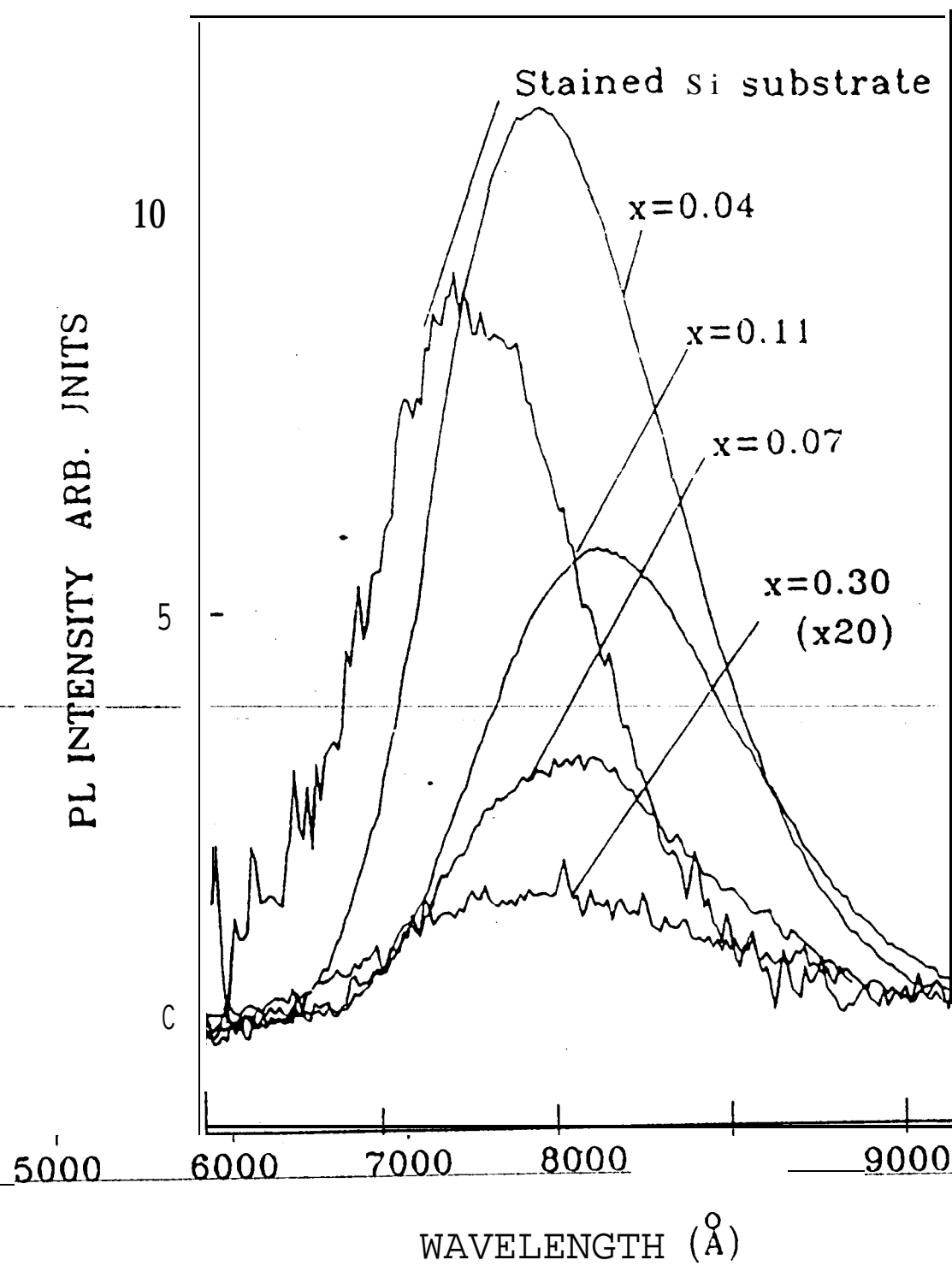


Fig 1